

Contents lists available at [ScienceDirect](http://www.sciencedirect.com)

Journal of Quantitative Spectroscopy & Radiative Transfer

journal homepage: www.elsevier.com/locate/jqsrt

Tuning near-field thermal radiative properties by quantifying sensitivity of Mie resonance-based metamaterial design parameters



Spencer J. Petersen^a, Soumyadipta Basu^b, Bart Raeymaekers^c,
Mathieu Francoeur^{a,*}

^a Radiative Energy Transfer Lab, Department of Mechanical Engineering, University of Utah, Salt Lake City, UT 84112, USA

^b Assembly Technology Development, Intel Corporation, Chandler, AZ 85226, USA

^c Nano-Tribology and Precision Engineering Laboratory, Department of Mechanical Engineering, University of Utah, Salt Lake City, UT 84112, USA

ARTICLE INFO

Article history:

Received 22 December 2012

Received in revised form

13 May 2013

Accepted 29 June 2013

Available online 9 July 2013

Keywords:

Near-field radiative transfer

Mie resonance-based metamaterials

Local density of electromagnetic states

ABSTRACT

The possibility of engineering near-field thermal radiative properties is investigated by adjusting design parameters of Mie resonance-based metamaterials. The sensitivities of surface polariton resonance frequencies, in both transverse magnetic and transverse electric polarizations, to parameters such as host medium relative permittivity and particle size and spacing (volume filling fraction) is determined. The sensitivity analysis is performed using a design of experiments method in combination with Mie resonance calculations and Clausius–Mossotti mixing relations. Particle size has the greatest effect on the resonance frequencies, while the volume filling fraction has the least. Based on the results from the sensitivity analysis, three metamaterials are selected for further analysis. The physics of these metamaterials is explored by calculating local density of electromagnetic states and surface polariton dispersion relation. As predicted by the sensitivity analysis, the local density of electromagnetic states and dispersion relation calculations show that Mie resonance-based metamaterials can be tuned to exhibit surface polariton resonance in the near-infrared spectrum. Energy density calculations show that surface polariton resonance in the near-infrared can be activated at temperatures as low as 800 K. Finally, a pathway to implementation of these metamaterials into macroscale engineering applications is proposed. Such metamaterials, with near-infrared surface polariton resonance, will significantly impact the development of nanoscale-gap thermophotovoltaic power generators for recycling waste heat into electricity.

© 2013 Elsevier Ltd. All rights reserved.

1. Introduction

Due to increasing worldwide energy demand, great interest has been placed in the development of low-cost high-efficiency renewable energy generation technologies [1]. Thermophotovoltaic (TPV) power generation is one such technology that converts radiative energy into

electric power via a TPV cell [2]. This is appealing as a renewable energy method because wasted heat can be recycled into usable power. When the separation between the radiator and the TPV cell is smaller than Wien's wavelength, radiation heat transfer enters the near-field regime [3–11]. In the near field, blackbody predictions can be exceeded by orders of magnitude as a result of evanescent wave tunneling. Also, resonant electromagnetic surface waves referred to as surface polaritons (SPs) can produce quasimonochromatic radiative transfer [12,13]. In addition to the inherent benefits of a TPV device

* Corresponding author. Tel.: +1 8015815721.

E-mail address: mfrancoeur@mech.utah.edu (M. Francoeur).

(quiet, low maintenance, nonpollutant, etc.), a nanoscale-gap TPV system capitalizing on the enhanced quasimonochromatic radiant energy exchange that occurs in the near field can significantly increase electrical energy generation. A number of theoretical [14–19] and experimental [20–22] analyses have been performed showing this enhanced energy exchange. A recent study has shown, however, that limitations are inherent with currently proposed nanoscale-gap TPV systems [23]. TPV cells have absorption bandgaps around 0.7 eV (1.8 μm), which is in the near-infrared (NIR) spectrum. Radiation at frequencies below the bandgap of a given cell is not sufficient to generate electron–hole pairs and results in thermal losses via absorption by the lattice and the free carriers. Similarly, excess radiative energy, greater than the bandgap, is also lost to heat by thermalization [23]. The resultant heating of the cell due to these aforementioned mechanisms, combined with heat dissipation via recombination of electron–hole pairs, induce a significant decrease in nanoscale-gap TPV power output and efficiency [23]. Therefore, it is imperative that a monochromatic radiation source in the NIR be found in order to develop viable, highly efficient nanoscale-gap TPV devices.

Biehls et al. [24], Joulain and Henkel [25], Ben-Abdallah et al. [26,27], Francoeur et al. [28–30], and Fu and Tan [31] have explored the possibility of tuning the frequency of SP driven monochromatic emission. They analyzed the near-field radiative exchange between various combinations of multilayered media, showing that, by varying layer thicknesses and compositions, near-field radiative emission can be spectrally tuned. Rodríguez et al. [32] analyzed the tunability of near-field emission via photonic crystals with various surface geometry patterns. Ilic et al. [33] showed that heat exchange by SPs can be tuned by varying manufacturing parameters of graphene. None of the materials studied in these works, however, demonstrated monochromatic NIR emission. West et al. [34] showed that conductive metal oxides are the only known material to sustain SP resonance in the NIR. However, their electromagnetic response depends heavily on the fabrication process. In summary, NIR resonance is rarely attained with naturally occurring materials.

Exotic properties that are not found in natural materials such as negative refractive index are attainable in electromagnetic metamaterials [35,36]. Metamaterials are artificial media consisting of subwavelength, customizable units, or “meta-atoms,” that manipulate incoming electromagnetic fields. Research applications that are significantly affected by the study of metamaterials include, but are not limited to, superlenses [36,37] and optical cloaking [36,38]. Customizing the electromagnetic properties of metamaterials makes possible the design of near-field thermal radiative properties, such as media exhibiting resonance in the NIR.

Joulain et al. [39] analyzed near-field radiative heat transfer between identical metamaterials consisting of arrays of metallic wires and split ring resonators. Similar studies were performed by Zheng and Xuan [40,41]. Basu and Francoeur [42] explored the penetration depth of near-field heat transfer when exchanged between two semi-infinite bulks of split ring resonator-wire metamaterial. All three groups showed that radiative heat exchange was

dominated by SPs in both transverse magnetic (TM) and transverse electric (TE) polarizations. This additional channel through which radiative energy transfer occurs (the TE-polarized SP) is a direct result of macroscale magnetic responses manifest in these metamaterials, which consist of microscopically nonmagnetic materials. No mention was made of tuning electromagnetic properties in any of these studies.

As an alternative to metal-based metamaterials, Mie resonance-based metamaterials are made up of particles within a host medium that manipulate incoming electromagnetic fields by scattering. Zhao et al. [43] performed theoretical analyses on metamaterials consisting of dielectric cubes made of a mixture of a ceramic material ($\text{Ba}_{0.5}\text{Sr}_{0.5}\text{TiO}_3$) and magnesium oxide in a Teflon host. Qiu and Gao [44] predicted radiative properties of metamaterials consisting of metallic-coated and uncoated dielectric nanospheres. The meta-atoms studied by both of these groups were arranged in ordered lattices. Wheeler et al. [45] showed experimentally that radiative properties can be customized via Mie resonance-based metamaterials with a random arrangement of dielectric particles. Since the meta-atoms are nothing more than particles and a host medium, the macroscopic electromagnetic properties of these metamaterials are isotropic. Additionally, the fabrication of Mie resonance-based metamaterials is potentially simpler than for metal-based metamaterials, as discussed at the end of this article.

Francoeur et al. [46] provided the first study in tuning near-field thermal properties of Mie resonance-based metamaterials where they considered silicon carbide nanoparticles within a potassium bromide host medium. Petersen et al. [47] performed local density of electromagnetic states (LDOS) calculations for the same metamaterial. Again, energy exchange was dominated by SPs in both TM and TE polarizations, showing that macroscale magnetic properties were manifest in these Mie resonance-based metamaterials. Recent studies have discussed the importance of high-permittivity, low-loss dielectric materials as candidates for metamaterial components with resonance in the infrared (IR) [45,48–55]. García-Etxarri et al. [56] addressed the possibility of employing silicon (Si) particles. In spite of the moderate permittivity of Si (~ 3.5) in the NIR, they were able to show that it is sufficient to induce resonances via a metamaterial made up of spherical Si particles with a radius $r_s = 200$ nm.

The objective of this work is to demonstrate the tunability of near-field thermal emission by Mie resonance-based metamaterials in the NIR bandwidth while showing the sensitivity of emission to adjustable metamaterial parameters, namely, particle diameter, host medium permittivity, and particle volume filling fraction. The metamaterials analyzed are made up of Si nanospheres. A design of experiments (DOE) analysis is performed to quantify the effects of varying each parameter on the SP resonance frequencies ω_r of the metamaterials. The effect of varying these parameters on the radiative properties is thoroughly explored by LDOS, SP dispersion relation, and energy density analyses on selected metamaterials.

A method for the direct calculation of near-field thermal emission by particulate media, e.g., Mie resonance-based metamaterials, is not currently found in the literature. Therefore, quantities such as LDOS and energy density are predicted in this paper using effective medium properties determined with the Clausius–Mossotti (CM) mixing relation. In spite of limiting assumptions in the formulation of the CM relation, the results will provide general trends and significant insights into SP resonance frequencies of metamaterials. Additionally, the results from these predictions will be beneficial when assessing the validity of the effective medium theory when direct calculation of near-field thermal emission by particulate media will be possible.

This paper is structured as follows. Following this introduction, the physical and mathematical description of the problem is given. Then, in the results section, three metamaterials are selected for further exploration based on the DOE analysis. LDOS, dispersion relation, and energy density calculations are performed on these three metamaterials and the results are discussed. In the fourth section, a technique for fabricating the Mie resonance-based metamaterials discussed in this paper is proposed. This technique is based on directed self-assembly using ultrasound waves. Finally, the results of the analyses are summarized in the conclusions.

2. Physical and mathematical description of the problem

Considered herein is an emitting bulk material in vacuum. The bulk is assumed semi-infinite with the bulk–vacuum (medium 1–medium 0) interface being smooth (see Fig. 1). Assuming a cylindrical coordinate system, the interface is azimuthally symmetric (along the θ direction) and infinite along the radial ρ direction. Therefore, results from these analyses depend solely on the z direction. The emitter is in local thermodynamic equilibrium and at temperature T_1 . Electromagnetic properties of the emitter are homogeneous, isotropic, and described by spatially local and frequency-dependent relative electric permittivity $\epsilon_1 (= \epsilon'_1 + i\epsilon''_1)$ and relative magnetic permeability $\mu_1 (= \mu'_1 + i\mu''_1)$. For convenience, from this point forward, the term “relative” will be omitted when referring to permittivity and permeability.

The thermal near field generated by the bulk at a distance Δ in vacuum, as shown in Fig. 1, is characterized by the energy density. The spectral energy density for

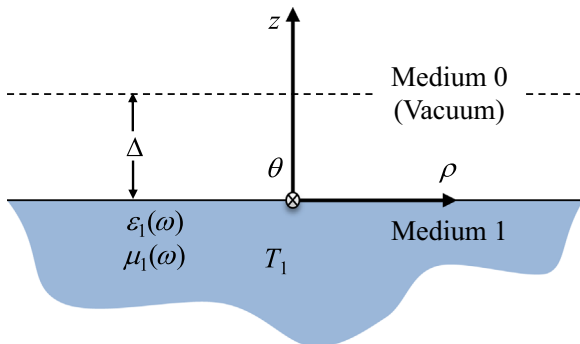


Fig. 1. Problem geometry and configuration.

media with arbitrary permittivity and permeability, derived from fluctuational electrodynamics, is [47]:

$$u_{\omega}(\Delta, T_1) = \frac{\Theta(\omega, T_1)}{4\pi^2 \omega} \left\{ k_v^2 \int_0^{k_v} \frac{k_{\rho} dk_{\rho}}{|k_{z0}|} \left[(1 - |r_{01}^{TM}|^2) + (1 - |r_{01}^{TE}|^2) \right] + 2 \int_{k_v}^{\infty} \frac{k_{\rho}^3 dk_{\rho}}{|k_{z0}|} [\text{Im}(r_{01}^{TM}) + \text{Im}(r_{01}^{TE})] e^{-2|k_{z0}|\Delta} \right\} \quad (1)$$

where k_v is the vacuum wavevector, k_{ρ} and k_z are respectively the parallel and normal components of the wavevector, while r_{01}^{TM} and r_{01}^{TE} are the medium 0–1 interface Fresnel reflection coefficients in TM and TE polarization, respectively. The spectral energy density can also be written as the product of the spectral LDOS $N_{\omega}(\Delta)$ and the mean energy of a Planck oscillator in thermal equilibrium $\Theta(\omega, T_1)$. Throughout these analyses, LDOS contributions from the emitting medium only are considered. LDOS contributions from free space and those reflected by the interface are intentionally omitted since the principal purpose of this work is to evaluate harvestable energy from the bulk. Just as the LDOS provides the possible energy that may be harvested from an emitting surface, the energy density quantifies the thermally activated energy for a specific temperature T_1 [4].

The emitting bulk is a Mie resonance-based metamaterial, defined by a number of parameters such as host permittivity and particle permittivity, size, size distribution, shape, orientation, arrangement, and spacing. The effective permittivity and permeability of the bulk are calculated using the scattering-corrected CM relations [57]:

$$\frac{\epsilon_1}{\epsilon_h} = 1 + N \left[\frac{k_h^3}{i6\pi} \left(\frac{1}{a_1} - 1 \right) - \frac{N}{3} \right]^{-1}, \quad (2a)$$

$$\frac{\mu_1}{\mu_h} = 1 + N \left[\frac{k_h^3}{i6\pi} \left(\frac{1}{b_1} - 1 \right) - \frac{N}{3} \right]^{-1} \quad (2b)$$

where ϵ_h and μ_h are, respectively, the permittivity and permeability of the host medium, $N (= 1/a^3)$ is the number of inclusions per unit volume, a is the lattice constant, k_h is the magnitude of the wavevector in the host medium, and a_1 and b_1 are the first order Mie scattering coefficients [58]. Wheeler has shown that, when within the long-wavelength regime, i.e., $\lambda_h \gg a > 2r_s$ with λ_h as the wavelength in the host medium, the permittivity and permeability can be considered isotropic [57]. Note that the CM model is only applicable to meta-atom configurations in which the volume filling fraction is significantly smaller than unity [36]. Effective medium calculations are the foundation of electromagnetic metamaterial studies as they draw from the microscale properties of the constituents to determine a macroscale homogeneous set of effective properties for the composite medium. However, at scales on the order of the meta-atom the effective medium approach loses accuracy, resulting in spatially dependent electromagnetic properties. Although such might be the case for near-field calculations, a full analysis of these spatial effects is beyond the scope of this work and is left to a future effort.

In this work, a number of metamaterial parameters are constrained, leaving three as variables for the sensitivity study. Si is selected as the particle material since it demonstrates moderate NIR permittivity and, thus, the potential for strong resonance in that bandwidth [56]. Note that over a large portion of the NIR spectrum, the complex refractive index of Si is obtained from the experimental work of Basu et al. [13]. At IR frequencies between 0.5×10^{15} and 3.5×10^{15} rad/s (0.5–3.8 μm) for which these data are lacking, properties from Palik [59] are used. Due to the assumptions of the CM model, the general geometric configuration of the meta-atom is fixed as spheres of uniform size arranged in a simple cubic lattice. The spacing, and hence the volume filling fraction, and size of the spheres are not fixed. In summary, host permittivity ϵ_h , sphere radius, and volume filling fraction F are selected as variable design parameters of a Mie resonance-based metamaterial.

Additionally, dispersion relation analyses are performed to understand the physics of an emitting metamaterial bulk. Petersen et al. [47] detailed the derivation of the SP dispersion relation that accounts for losses in the emitter for both polarization states. The following conditions apply to TM polarized SP dispersion:

1. $n'_1 n''_1$ must be close to zero,
2. ϵ'_1 must be close to zero,
3. the tangential wavevector k_p , must be defined as

$$k_p^2 = k_v^2 \frac{\epsilon'^2_1 n''^2_0 - \epsilon''^2_0 (n'^2_1 - n''^2_1)}{\epsilon'^2_1 - \epsilon''^2_0}, \quad (3)$$

4. and, for emitting into vacuum,

$$\epsilon'_1 < -1 \text{ and } n'^2_1 - n''^2_1 < 1 \quad (4a)$$

or

$$-1 < \epsilon'_1 < 0 \text{ and } n'^2_1 - n''^2_1 > 1 \quad (4b)$$

where $n_i (= n'_i + in''_i = \sqrt{\epsilon_i \mu_i})$ is the refractive index of medium i and $\epsilon_0 (=1)$ is the vacuum permittivity. Note that the above discussion is equally applicable for TE polarized SPs when ϵ terms are replaced with μ .

The most significant contribution to near-field energy exchange emerges from the resonance of SPs when $|dk_p/d\omega| \rightarrow \infty$ where ω is the angular frequency. The denominator of Eq. (3) shows that this occurs when $\epsilon'_1 = -1$ (or when $\mu'_1 = -1$ for TE polarization). However, conditions 1 and 2 also state that the losses must be small for SPs to exist and, hence, for resonance to occur.

3. Results

3.1. Design of experiments

The primary intent of this work is to explore the sensitivity of Mie resonance-based metamaterial design parameters on the TM and TE polarized SP resonance frequencies $\omega_{r, TM}$ and $\omega_{r, TE}$, respectively. DOE is often used to determine the effects of input variation on a set of experiments. As discussed in Section 2, the variable inputs for this sensitivity study are sphere radius, host

permittivity, and volume filling fraction and the experiments are theoretical calculations of SP resonance frequencies. These calculations are carried out by first using Mie coefficients and the CM mixing equations to predict the effective permittivity and permeability of the metamaterial

(Eqs. (2a) and (2b)). With the effective properties known, the resonance frequencies are determined by locating where, for TM polarization, $\epsilon'_1 = -1$ and $n'_1 n''_1$ and ϵ''_1 are small and, for TE polarization, $\mu'_1 = -1$ and $n'_1 n''_1$ and μ''_1 are small.

It is important to note that these effective medium calculations are meant to establish only a first order projection of the relationship between the variable inputs and the SP resonance frequencies. Since, as mentioned above, only the first order Mie coefficients for Si spheres are employed in the DOE analysis. Higher order Mie coefficients are required to accurately predict the electromagnetic response of a sphere the size of which is similar to the field wavelength. Hence, the more detailed LDOS analyses, described in Section 3.2, include a thorough review of the higher order Mie coefficients to maximize the accuracy of the results.

Since a DOE analysis includes calculating the variation of an output due to the perturbation of its inputs, ranges must be established for each of the input variables. A minimum sphere radius of 141 nm is selected since it is the smallest sphere radius that produces a resonance within the NIR spectral band ($0.75\text{--}2.51 \times 10^{15}$ rad/s or 0.75–2.50 μm). A maximum sphere radius of 500 nm is near the largest size of Si spheres that is easily procured from current nanoparticle suppliers. Larger Si spheres are manufacturable, but at considerable cost and effort. A volume filling fraction range of from 0.1 to 0.4 is chosen to thoroughly explore the limits of the CM mixing equations. The host permittivity ranges from 1 (that of vacuum) to 5.96, which is the maximum that results in a NIR resonance.

The only information extracted from the DOE analysis is the main effects, i.e., the sensitivity of the three metamaterial design parameters on the SP resonances. The main effect of a given design parameter is the average change in predicted resonance frequency for all other design parameter combinations in which the given parameter changes from its minimum to its maximum [60]. For example, the main effect of sphere radius on TM resonance is the average change in TM resonance accompanying a change in sphere radius from 141 (minimum) to 500 nm (maximum) over four separate cases: (i) $\epsilon_h = 1.00$ (minimum) and $F = 0.1$ (minimum); (ii) $\epsilon_h = 1.00$ (minimum) and $F = 0.4$ (maximum); (iii) $\epsilon_h = 5.96$ (maximum) and $F = 0.1$ (minimum); (iv) $\epsilon_h = 5.96$ (maximum) and $F = 0.4$ (maximum). The 2^3 factorial analysis is a form of DOE analysis that involves calculating every combination of the maxima and minima of three variable design parameters, making the total number of resonance predictions eight ($=2^3$). This combination of predictions provides sufficient data to successfully evaluate the main effects as defined above.

For each of the three metamaterial parameters, main effects for both the TM and TE SP resonances are calculated. Table 1 shows the results for the TM and TE predictions. The larger the magnitude of the main effect,

the more strongly the design parameter correlates with the resonance frequency. A negative main effects value implies that the resonance, on average, decreases with an increase in the design parameter. As can be seen in Table 1, sphere radius has the most significant effect on the resonance in both polarizations. Conversely, the effect of the filling fraction is two orders of magnitude smaller than that of the sphere radius. For TM polarization, both volume filling fraction and host permittivity show main effects nearly two orders of magnitude smaller than sphere radius. The host medium permittivity has a greater influence on the TM resonance than on the TE.

Since the sensitivity to the volume filling fraction is relatively small, the resonances can be visualized with two-dimensional surface contours as functions of sphere radius and host medium permittivity. Six sphere radii and six host permittivities (making $6^2=36$ resonance calculations for each polarization) equally-spaced within the ranges specified for the DOE analysis are analyzed and charted as the response surfaces. The volume filling fraction for these calculations is held at 0.4. The surfaces are shown in Fig. 2.

As seen in Fig. 2, the TM polarized SP resonance frequency is less affected by variations in the host permittivity than the TE, which is also observed in Table 1. Figure 2 shows that the sphere radius is the most significant contributor to the tunability of resonance frequencies in the metamaterial. At a host relative permittivity of about 4.5, an overlap occurs where both TM and TE resonances appear at the same frequency. This overlap is also relatively independent of sphere radius.

Using the results from the DOE analysis, three metamaterials of interest are selected for further exploration.

Table 1
Results of TM and TE polarized SP resonance frequency DOE analysis.

Design parameter	TM main effect (rad/s)	TE main effect (rad/s)
Sphere radius r_s	-1.39×10^{15}	-1.10×10^{15}
Volume filling fraction F	-2.30×10^{13}	2.16×10^{13}
Host medium permittivity ϵ_h	-6.20×10^{13}	2.79×10^{14}

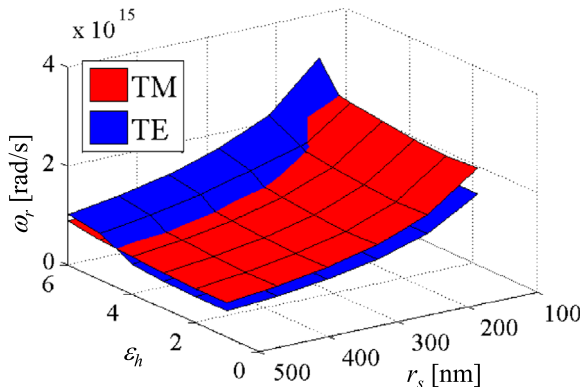


Fig. 2. TM and TE polarized SP resonance frequency as functions of sphere radius and host medium permittivity.

These metamaterials are strategically selected to further prove, with a more in-depth analysis, two of the conclusions from the sensitivity analysis: the volume filling fraction is weakly correlated with the SP resonance frequency and the sphere radius strongly. Metamaterial #1 is made up of 230-nm radius particles within a theoretical nonmagnetic host medium with a permittivity of 1.0; the volume filling fraction is 0.4. The particles in Metamaterial #2 are also 230 nm in radius. The host permittivity is also 1.0 and the volume filling fraction 0.1. Metamaterial #3 consists of 150-nm radius particles in a host of permittivity 1.0 with a volume filling fraction of 0.4. To better understand the physics of what is predicted by the effective property calculations, LDOS and dispersion relation analyses are performed on these three metamaterials.

It is important to note that a large number of metamaterials described by the contours shown in Fig. 2 should not be further analyzed unless a method is employed that accounts for multipole phenomena. These metamaterials result in significant higher order Mie coefficients that render the CM mixing relation insufficient as it is described herein. Among said metamaterials are those aligned with the TE and TM polarized SP resonance frequency overlap at $\epsilon_h \sim 4.5$.

3.2. LDOS calculations

In this section, the aforementioned metamaterials are analyzed further via LDOS profiles. Higher order Si sphere Mie coefficients are thoroughly reviewed for each of the metamaterials to justify the use of only the first order coefficients in Eqs. (2a) and (2b). According to the criteria for the existence of SPs listed in Section 2, dispersion relation analyses are also performed [47]. Results are overlaid with the spectral LDOS per unit tangential wavevector $N_\omega(k_\rho)$. The maximum allowable wavevector for electromagnetic waves in amorphous Si, based on the approximate atomic spacing of 2.7 Å, is 3.7×10^9 rad/m [61,62]. All data presented herein fall below this critical value.

3.2.1. Metamaterial #1

The spectral LDOS per unit tangential wavevector (at $\Delta=50$ nm) and dispersion relation for Metamaterial #1 are shown in Fig. 3(a), while the spectral LDOS (integrated over all tangential wavevectors) are shown in Fig. 3(b). The vacuum light line is compared to the metamaterial light line and the dispersion relation (Eq. (3)) for TE polarized SPs $k_{\rho,TE}$. Note that the emitter and vacuum light lines k_e and k_v , respectively, are included in the analysis to delineate the different wave modes at the interface 1–0. Assume the vacuum light line is smaller than that of the emitter. Waves found to the left of the vacuum light line are propagating on both sides of the interface. Total internal reflection (TIR) occurs between the vacuum and metamaterial light lines, where evanescent waves are found on the vacuum side and reflected propagating waves on the emitter side of the interface. Waves are evanescent on both sides of the interface when located to the right of the emitter light line, where SPs may exist.

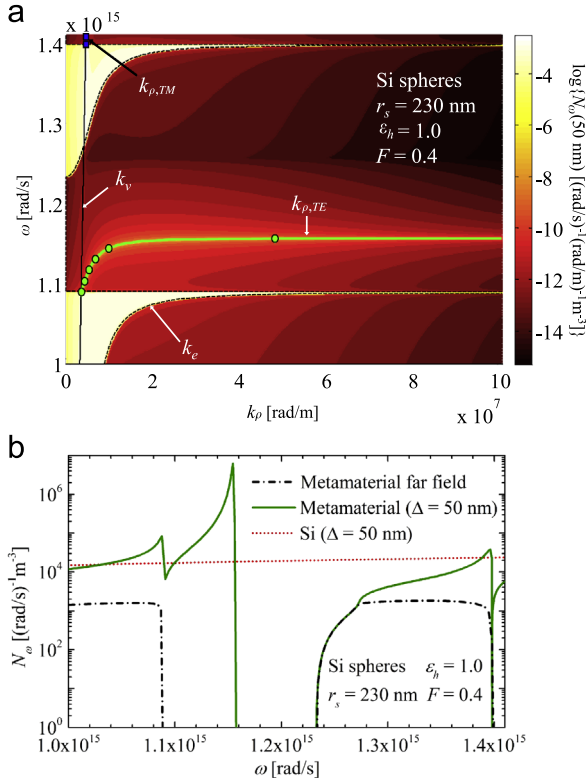


Fig. 3. (a) Metamaterial #1 spectral LDOS per unit tangential wavevector at $\Delta=50$ nm and SP dispersion relation. (b) Metamaterial #1 spectral LDOS. Near- (green solid) and far-field (black dash-dot) spectra for the metamaterial are compared to the near-field spectra of a Si bulk (red dot). (For interpretation of the references to color in this figure legend, the reader is referred to the web version of this article.)

Finally, TIR is not possible if the vacuum light line is greater than the emitter light line.

Figure 4 shows the spectral distribution of the first and second order Mie coefficients (a_1 , b_1 , a_2 , and b_2) for a 230-nm Si sphere between 1.00×10^{15} and 1.41×10^{15} rad/s (1.88 and 1.34 μm). The first order Mie coefficient b_1 reaches a maximum at 1.13×10^{15} rad/s, which coincides well with the TE polarized SP resonance frequency found at 1.16×10^{15} rad/s. Over this spectral band, the second order coefficients (a_2 and b_2) are never more than 10% of the first order coefficients, showing that higher order contributions to Eqs. (2a) and (2b) can be neglected.

As seen in Fig. 3(a), horizontal quasiasymptotes in the metamaterial light line at 1.09×10^{15} and 1.40×10^{15} rad/s (1.73 and 1.35 μm) result in significant LDOS due to TIR. The prefix “quasi” is used since the dispersion relation analysis conducted herein accounts for losses and an infinite wavevector is impossible in a lossy medium. A potential NIR resonance frequency is shown at 1.16×10^{15} rad/s (1.62 μm) where the TE polarized SP dispersion relation reaches a quasiasymptote. A close inspection of the losses for this metamaterial (see Fig. 5) shows that the quasiasymptote at 1.16×10^{15} rad/s is indeed SP-driven since μ_1'' and $n_1' n_1''$ are close to zero (2.07×10^{-9} and 5.88×10^{-10} , respectively) at that frequency. Immediately neighboring the TIR region that

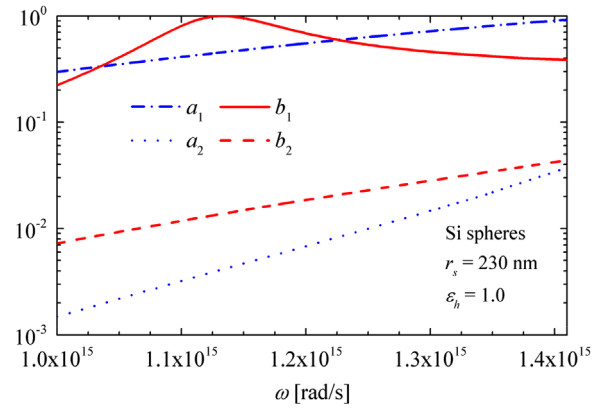


Fig. 4. Metamaterial #1 spectral first and second order Mie coefficients.

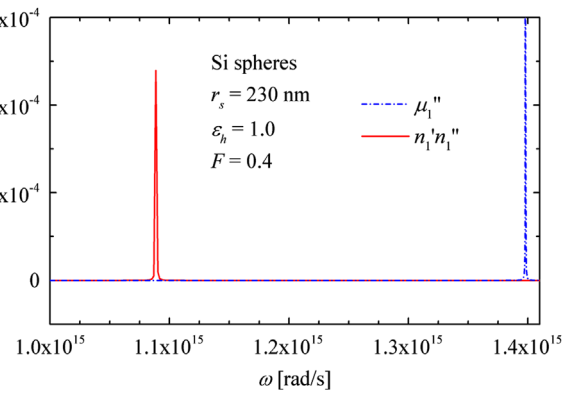


Fig. 5. Metamaterial #1 losses.

peaks at 1.40×10^{15} rad/s is a grouping of TM polarized SPs that do not reach a resonance within this spectral band.

Near- (at $\Delta=50$ nm) and far-field spectral LDOS are compared with near-field LDOS (also at $\Delta=50$ nm) for a Si bulk in Fig. 3(b). At 50 nm, the metamaterial shows a significant LDOS peak at 1.16×10^{15} rad/s, which agrees perfectly with the resonance frequency calculated by the dispersion relation analysis (see Fig. 3(a)). This peak is accompanied by a smaller local maximum, which aligns with one of the TIR regions in Fig. 3(a). The far-field LDOS distribution is smaller over the entire bandwidth, as expected, since evanescent waves do not contribute to the electromagnetic states at large distances from the emitter. Within the SP bandwidth, the far-field LDOS is negligible. A close observation of the Si distribution relative to that of the metamaterial shows how much near-field energy exchange enhancement is possible due to metamaterial sustained SPs.

3.2.2. Metamaterial #2

The SP dispersion relation and spectral LDOS per unit tangential wavevector (at $\Delta=50$ nm) for Metamaterial #2 are shown in Fig. 6(a). A SP dispersion relation quasiasymptote is seen at 1.14×10^{15} rad/s (1.65 μm) in TE polarization. The losses for this metamaterial are small at this frequency ($\mu_1'' = 1.00 \times 10^{-8}$, $n_1' n_1'' = 6.98 \times 10^{-9}$); therefore,

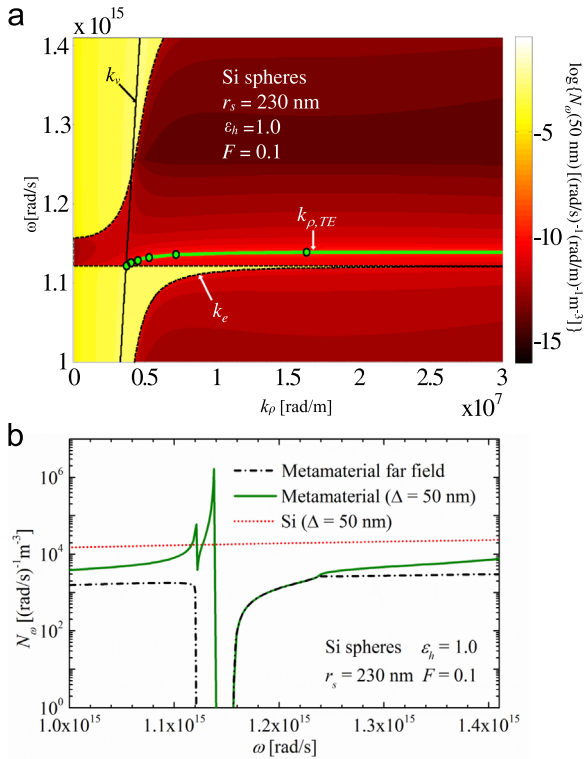


Fig. 6. (a) Metamaterial #2 spectral LDOS per unit tangential wavevector at $\Delta=50$ nm and SP dispersion relation. (b) Metamaterial #2 spectral LDOS. Near- (green solid) and far-field (black dash-dot) spectra for the metamaterial are compared to the near-field spectra of a Si bulk (red dot). (For interpretation of the references to color in this figure legend, the reader is referred to the web version of this article.)

it is deemed a SP resonance. A horizontal quasiasymptote in the metamaterial light line at 1.12×10^{15} rad/s aligns with significant LDOS due to TIR and is adjacent to the SP resonance. As previously stated, the first order Mie coefficient b_1 for a 230-nm Si sphere is maximum at 1.13×10^{15} rad/s, which is closely aligned with the TE polarized SP resonances of both Metamaterial #1 (1.16×10^{15} rad/s) and #2 (1.14×10^{15} rad/s). The slight discrepancy between Metamaterials #1 and #2 indicates that, although the Mie coefficients drive the predictions, applying the CM mixing relation results in amplification of the resonance frequencies. Also mentioned previously, second order Mie coefficients are no more than 10% of the first order coefficients within this spectral band.

The Metamaterial #2 spectral LDOS for both the near (at $\Delta=50$ nm) and far field is shown in Fig. 6(b) and compared with that of a Si bulk at 50 nm. A significant peak in the metamaterial near-field LDOS is found at 1.14×10^{15} rad/s, which agrees perfectly with the resonance predictions from the dispersion relation analysis (see Fig. 6(a)). Metamaterial #1 exhibits SP resonance at nearly the same frequency $\sim 1.16 \times 10^{15}$ rad/s (see Fig. 3(b)), further proving that the volume filling fraction has little effect on the SP resonance since the only configurational difference between Metamaterials #1 and #2 is the volume fraction (0.4 and 0.1, respectively). A smaller local maximum accompanies this resonance peak

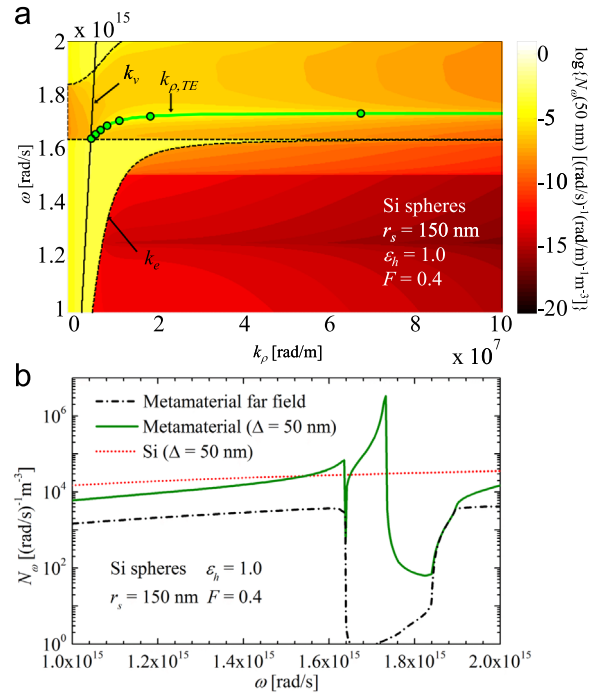


Fig. 7. (a) Metamaterial #3 spectral LDOS per unit tangential wavevector at $\Delta=50$ nm and SP dispersion relation. (b) Metamaterial #3 spectral LDOS. Near- (green solid) and far-field (black dash-dot) spectra for the metamaterial are compared to the near-field spectra of a Si bulk (red dot). (For interpretation of the references to color in this figure legend, the reader is referred to the web version of this article.)

at 1.12×10^{15} rad/s, which aligns with the TIR region seen in Fig. 6(a). Far-field LDOS is smaller than that of the near field and at all SP frequencies is negligible. A comparison between the Si and metamaterial LDOS distributions again shows the possible marked improvements to near-field energy exchange by Mie resonance-based metamaterials

3.2.3. Metamaterial #3

Figure 7(a) charts the spectral LDOS per unit tangential wavevector (at $\Delta=50$ nm) and SP dispersion relation for Metamaterial #3. A horizontal quasiasymptote is found on the metamaterial light line at 1.64×10^{15} rad/s ($1.15 \mu\text{m}$), where significant LDOS due to TIR is also found. A SP dispersion relation quasiasymptote found at 1.73×10^{15} rad/s ($1.09 \mu\text{m}$) corresponds with small losses ($\mu_1' = 3.71 \times 10^{-4}$, $n_1' n_1'' = 6.54 \times 10^{-4}$), making it a true SP resonance. The first order Mie coefficient b_1 for a 150-nm Si sphere reaches a maximum at 1.70×10^{15} rad/s, which is closely aligned with this TE polarized SP resonance. Higher order 150-nm Si sphere Mie coefficients are small enough, relative to the first order coefficients, that their contribution is negligible over this spectral band. Neither the spectral losses nor higher order Mie coefficients are shown herein.

Spectral LDOS for Metamaterial #3 in the far field and at 50 nm are compared to that of a Si bulk at 50 nm in Fig. 7(b). A significant near-field LDOS peak for the metamaterial is found at 1.73×10^{15} rad/s, which aligns with the dispersion relation analysis resonance prediction (see Fig. 7(a)). A more

significant change in the SP resonance frequency with respect to Metamaterial #1 (1.16×10^{15} rad/s—see Fig. 3(b)) is evident with Metamaterial #3 than with #2 (1.14×10^{15} rad/s—see Fig. 6(b)), showing that the sphere radius has a larger effect on the SP resonance frequency than the volume fraction. A smaller local maximum at 1.64×10^{15} rad/s aligns well with the emitter light line horizontal quasiasymptote in the dispersion relation and is attributed to TIR. The far-field metamaterial LDOS is again negligible over the SP domain. Outside of the SP domain, the metamaterial maintains far-field LDOS markedly smaller than in the near field as expected. The Si bulk shows near-field LDOS similar to but only slightly smaller than the metamaterial over the majority of the bandwidth since, with such a relatively large volume fraction of Si particles, the metamaterial is expected to approach the characteristics of bulk Si. The only exception to this observation is within the SP and TIR regions, where near-field effects dominate the LDOS.

An additional exploration of Metamaterial #3 is conducted by calculating the energy density to examine the temperature dependence on thermal activation of the nearly monochromatic TE polarized SP resonances discussed above. Figure 8 shows the energy density of Metamaterial #3 for $T_1=700, 800,$ and 900 K with $\Delta=50$ nm. At 700 K, the peak energy density is at the edge of the spectral band, 1.00×10^{15} rad/s ($1.88 \mu\text{m}$). The SP resonance at 1.73×10^{15} rad/s is not significantly activated at this temperature. When the temperature is increased to 800 K, the SP resonance barely dominates the density spectra, overcoming the local maximum found at 1.00×10^{15} rad/s. By the time the temperature reaches 900 K, the local peak at 1.00×10^{15} rad/s is completely drowned out by the resonance by almost a factor of three. Without the resonance – that is now shown to be easily tuned using Mie resonance-based metamaterials – thermal activation of 1.73×10^{15} rad/s would not occur until $T_1=2660$ K. A low-temperature NIR resonance such as this will significantly impact nanoscale-gap TPV power generation, as it can allow for electrical power generation by these devices at temperatures 1760 K lower than with commonly employed materials.

A close inspection of the distributions in Figs. 3(a), 6(a), and 7(a) reveals that the immense LDOS values surrounding the SP dispersion relations are barely visually

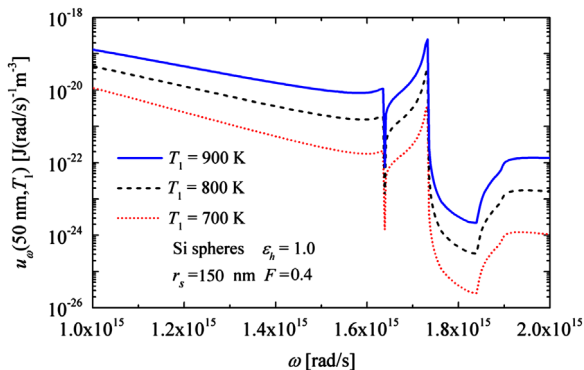


Fig. 8. Metamaterial #3 energy density spectra at $T_1=700, 800,$ and 900 K.

perceivable. In other words, a large, narrow peak of LDOS follows these dispersion curves. In order to generate the corresponding spectral distributions shown in Figs. 3(b), 6(b), 7(b), and 8, integration over all tangential wavevectors in Figs. 3(a), 6(a), and 7(a) is required (see Eq. (1)). Since the LDOS peaks are so narrow near the SP dispersion, a standard discretization scheme, starting with $k_p=0$, marching toward $k_p \rightarrow \infty$, with a small Δk_p , proves extremely inefficient. Unless Δk_p is dramatically small, which significantly effects the computation time, the entire LDOS peak is overlooked. To both mitigate this inaccuracy and decrease computation time, the integrations are performed starting at the LDOS peak maxima (according to the SP dispersion relation (Eq. (3))), marching outwards, in both directions, until convergence.

4. Fabrication of Mie resonance-based metamaterials

To take advantage of the exotic properties of Mie resonance-based metamaterials in real engineering applications, fabrication of macroscale specimens is necessary. Very few experimental works have been reported in the literature that demonstrate fabrication of dielectric metamaterials. Schuller et al. [53] measured IR extinction spectra of single whisker-shaped silicon carbide particles, and identified three resonant modes. The authors showed that these modes may be employed for designing dielectric-based metamaterials with negative index of refraction. Wheeler et al. [45,57] performed IR measurements on metamaterial samples prepared by mixing silicon carbide and potassium bromide powders pressed into a pellet. The reflectance spectrum, in good agreement with the theoretical predictions, showed that the metamaterial exhibits electric and magnetic resonances in the IR. Ginn et al. [63] measured transmittance and reflectance of metamaterials made of tellurium cubic inclusions coated on a film. The samples were fabricated using lithography techniques. However, none of the fabricated samples described in [45,53,57,63] can be used for real engineering applications because of scale and other restrictions. Electron beam lithography [64] has also been suggested as a fabrication technique for dielectric-based metamaterials. This technique allows covering a macroscale area, but the thickness of the resulting samples is limited. Increasing the thickness requires accurate alignment between different individual layers of material subsequently deposited. Furthermore, it was suggested that fabrication techniques used for metamaterials with metallic inclusions [65] are transferrable to the fabrication of dielectric (Mie resonance-based) metamaterials, such as interferometric lithography [66], and two photon polymerization [64]. A careful review of recent literature shows that no demonstration of macroscale (volume) dielectric metamaterial fabrication exists.

A novel method to manufacture macroscale metamaterial specimens is proposed here. This approach promises a solution for the scalability limitation of existing fabrication methods, and is based on the acoustic radiation force associated with a standing pressure wave. Gor'kov [67] showed that in an inviscid medium, the acoustic radiation force acting on a spherical particle with radius R can be

expressed as the negative gradient of the force potential $F = -\nabla U$ for an arbitrary direction x :

$$F_x = \frac{\pi R^3}{3} p_{0x}^2 k_x \beta_m \phi \sin(2k_x x), \quad (5)$$

where p_{0x} is the peak pressure amplitude, $k_x = 2\pi/\lambda_x$, is the wave number, and λ_x is wavelength in the x -direction. $\beta_m = 1/\rho_m c_m^2$ is the compressibility of the medium, ρ_m and c_m are the density and the sound propagation velocity of the medium. The subscript x refers to the propagation direction of the wave. As a result of the acoustic radiation force, particles are driven towards the nodes ($\Phi > 0$) or the antinodes ($\Phi < 0$) of the standing pressure wave [68]. Φ is the acoustic contrast factor given by

$$\Phi = \frac{5\rho_p - 2\rho_m}{2\rho_p + \rho_m} \frac{\beta_p}{\beta_m}, \quad (6)$$

where $\beta_p = 1/\rho_p c_p^2$ is the compressibility, ρ_p the density, and c_p the sound propagation velocity of the spherical particle.

Using three orthogonal resonators, piezoelectric crystals in this instance, a 3D standing wave pattern can be established in a square reservoir containing a dispersed solution of particles and a polymer host medium. The 3D standing wave pattern can be designed to match the designs of the metamaterials described in Sections 2 and 3 of this paper. The acoustic radiation force associated with the ultrasound standing wave pattern drives the dispersed particles to the nodes of the interference pattern where they accumulate. This has previously been demonstrated in Ref. [69] and is conceptually illustrated in Fig. 9. When the particles have accumulated at the nodes of the standing wave interference pattern, the polymer is cross-linked to fixate the clusters of particles in place, constituting a macroscale Mie resonance-based metamaterial.

5. Conclusions

The tunability of the electromagnetic properties of Mie resonance-based metamaterials is demonstrated. A DOE analysis is conducted to quantify the sensitivity of adjustable metamaterial design parameters, i.e., particle size and spacing and host permittivity, on TM and TE polarized SP resonances. The DOE analysis, in conjunction with Mie resonance calculations and CM mixing relations, shows that particle size has the greatest effect on resonance frequencies by nearly an order of magnitude. When host

permittivity is approximately 4.5, TM and TE polarized SP resonances are found at the same frequency.

Three metamaterials are selected from the results of the sensitivity analysis to further explore their near-field physics. LDOS and SP dispersion relation analyses are performed on these metamaterials to confirm the existence of resonance conditions. NIR resonance frequencies in TE polarization are found with these metamaterials at 1.14×10^{15} , 1.16×10^{15} and 1.73×10^{15} rad/s. The two metamaterials showing nearly identical SP resonances (#1 at 1.16×10^{15} and #2 at 1.14×10^{15} rad/s) differed only by volume filling fraction (0.4 and 0.1, respectively). Metamaterial #3 shows a different resonance frequency at 1.73×10^{15} rad/s and differs from the other two by the sphere radius (150 nm for #3 vs. 230 nm for #1 and #2). These results further prove the conclusions set forth by the DOE analysis that the volume filling fraction has little effect on the SP resonance while the sphere radius has a larger effect.

One of the Mie resonance-based metamaterials studied in this paper demonstrates thermally activated SP resonance at temperatures more than 1700 K lower than in Si. This metamaterial shows a SP resonance in the NIR that is activated at 800 K, dominating the spectral distribution of energy density. Without the SP resonance, a dominant energy density in the NIR does not occur until 2660 K.

The results presented in this paper show that near-field radiative properties of Mie resonance-based metamaterials are tunable by adjusting design parameters such as host permittivity and particle size and spacing. A fabrication method is proposed for implementing these metamaterial designs in macroscale engineering applications. And, with the advent of these metamaterials in the fabrication of nanoscale energy devices, SP resonances can be tuned to within the NIR, making monochromatic energy transfer available at temperatures as low as 800 K.

The validity of the effective medium theory technique employed in these analyses, the CM mixing relation, is questionable in the near field of metamaterials. However, this approach is the only method currently available for predicting near-field thermal emission by particulate media. SP resonance frequency trends presented herein will provide significant insight into near-field capabilities of thermally emitting metamaterials. Additionally, these results will aid in assessing the validity of the effective medium theory when direct calculation of near-field thermal emission by particulate media will be tractable.

Acknowledgments

This work was partially sponsored by the National Science Foundation under Grant no. DMR 11-21252.

References

- [1] Baxter J, Bian Z, Chen G, Danielson D, Dresselhaus MS, Fedorov AG, et al. *Energy Environ Sci* 2009;2:559–88.
- [2] Bauer T. *Thermophotovoltaics: basic principles and critical aspects of system design*. Berlin: Springer; 2011.
- [3] Joulain K, Mulet J-P, Marquier F, Carminati R, Greffet J-J. *Surf Sci Rep* 2005;57:59–112.

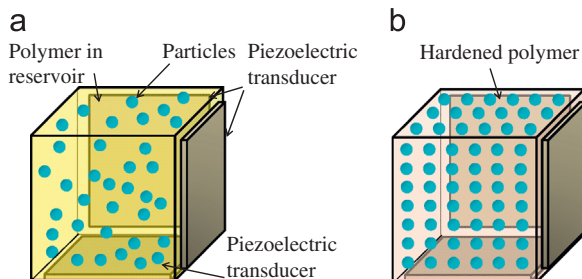


Fig. 9. 3D macroscale metamaterial fabrication technique based on ultrasound standing pressure waves.

- [4] Zhang ZM. Nano/microscale heat transfer. New York: McGraw-Hill; 2007.
- [5] Hu L, Narayanaswamy A, Chen X, Chen G. Appl Phys Lett 2008;92:133106.
- [6] Basu S, Zhang ZM, Fu CJ. Int J Energy Res 2009;33:1203–32.
- [7] Rousseau E, Siria A, Jourdan G, Volz S, Comin F, Chevrier J, et al. Nat Photonics 2009;3:514–7.
- [8] Shen S, Narayanaswamy A, Chen G. Nano Lett 2009;9:2909–13.
- [9] Howell JR, Siegel R, Mengüç P. Thermal radiation heat transfer. 5th ed. Boca Raton: CRC Press; 2011.
- [10] Ottens RS, Quetschke V, Wise S, Alemi AA, Lundock R, Mueller G, et al. Phys Rev Lett 2011;107:014301.
- [11] Shen S, Mavrokefalos A, Sambegoro P, Chen G. Appl Phys Lett 2012;100:133114.
- [12] Mulet J-P, Joulain K, Carminati R, Greffet J-J. Microscale Therm Eng 2002;6:209–22.
- [13] Basu S, Lee BJ, Zhang ZM. J Heat Transfer 2010;132:023301.
- [14] Whale MD. [Ph.D. dissertation]. Massachusetts Institute of Technology, 1997.
- [15] Whale MD, Cravalho EG. IEEE Trans Energy Convers 2002;17:130–42.
- [16] Narayanaswamy A, Chen G. Appl Phys Lett 2003;82:3544–6.
- [17] Laroche M, Carminati R, Greffet J-J. J Appl Phys 2006;100:063704.
- [18] Park K, Basu S, King WP, Zhang ZM. J Quant Spectrosc Radiat Transfer 2008;109:305–16.
- [19] Ilic O, Jablan M, Joannopoulos JD, Celanovic I, Soljačić M. Opt Express 2012;20:A366–84.
- [20] DiMatteo RS, Greiff P, Finberg SL, Young-Waithe KA, Choy HKH, Masaki MM, et al. Appl Phys Lett 2001;79:1894–6.
- [21] DiMatteo RS, Greiff P, Seltzer D, Meulenber G, Brown E, Carlen E, et al. AIP Conf Proc 2004;738:42–51.
- [22] Hanamura K, Mori K. AIP Conf Proc 2007;890:291–6.
- [23] Francoeur M, Vaillon R, Mengüç MP. IEEE Trans Energy Convers 2011;26:686–98.
- [24] Biehs S-A, Reddig D, Holthaus M. Eur Phys J B 2007;55:237–51.
- [25] Joulain K, Henkel C. Appl Phys B—Lasers Opt 2008;93:151–8.
- [26] Ben-Abdallah P, Joulain K, Drevillon J, Domingues G. Appl Phys Lett 2009;94:153117.
- [27] Ben-Abdallah P, Joulain K, Drevillon J, Domingues G. J Appl Phys 2009;106:044306.
- [28] Francoeur M, Mengüç MP, Vaillon R. Appl Phys Lett 2008;93:043109.
- [29] Francoeur M, Mengüç MP, Vaillon R. J Appl Phys 2010;107:034313.
- [30] Francoeur M, Mengüç MP, Vaillon R. J Phys D Appl Phys 2010;43:075501.
- [31] Fu CJ, Tan WC. J Quant Spectrosc Radiat Transfer 2009;110:1027–36.
- [32] Rodríguez AW, Ilic O, Bermel P, Celanovic I, Joannopoulos JD, Soljačić M, et al. Phys Rev Lett 2011;107:114302.
- [33] Ilic O, Jablan M, Joannopoulos JD, Celanovic I, Buljan H, Soljačić M. Phys Rev B 2012;85:155422.
- [34] West PR, Ishii S, Naik GV, Emani NK, Shalaev VM, Boltasseva A. Laser Photonics Rev 2010;1–13:795–808.
- [35] Veselago VG. Sov Phys—Usp 1968;10:509–14.
- [36] Cai W, Shalaev V. Optical metamaterials: fundamentals and applications. New York: Springer; 2010.
- [37] Pendry JB. Phys Rev Lett 2000;85:3966–9.
- [38] Pendry JB, Schurig D, Smith DR. Science 2006;312:1780–2.
- [39] Joulain K, Drevillon J, Ben-Abdallah P. Phys Rev B 2010;81:165119.
- [40] Zheng Z, Xuan Y. Int J Heat Mass Transfer 2011;54:1101–10.
- [41] Zheng Z, Xuan Y. Chin Sci Bull 2011;56:2312–9.
- [42] Basu S, Francoeur M. Appl Phys Lett 2011;99:143107.
- [43] Zhao Q, Kang L, Du B, Zhao H-J, Xie Q, Li B, et al. Chin Sci Bull 2008;53:3272–6.
- [44] Qiu C-W, Gao L. J Opt Soc Am B 2008;25:1728–37.
- [45] Wheeler MS, Aitchison JS, Chen JLL, Ozin GA, Mojahedi M. Phys Rev B 2009;79:073103.
- [46] Francoeur M, Basu S, Petersen S. Opt Express 2011;19:18774–88.
- [47] Petersen SJ, Basu S, Francoeur M. Photonic Nanostruct 2013. <http://dx.doi.org/10.1016/j.photonics.2013.03.002>, in press.
- [48] Huang KC, Povinelli ML, Joannopoulos JD. Appl Phys Lett 2004;85:543–5.
- [49] Wheeler MS, Aitchison JS, Mojahedi M. Phys Rev B 2005;72:193103.
- [50] Yannopapas V, Moroz A. J Phys: Condens Matter 2005;17:3717–34.
- [51] Jylhä L, Kolmakov I, Maslovski S, Tretyakov S. J Appl Phys 2006;99:043102.
- [52] Peng L, Ran L, Chen H, Zhang H, Kong JA, Grzegorzczak TM. Phys Rev Lett 2007;98:157403.
- [53] Schuller JA, Zia R, Taubner T, Brongersma ML. Phys Rev Lett 2007;99:107401.
- [54] Ahmadi A, Mosallaei H. Phys Rev B 2008;77:045104.
- [55] Vynck K, Felbacq D, Centeno E, Dabuz AI, Cassagne D, Guizal B. Phys Rev Lett 2009;102:133901.
- [56] García-Etxarri A, Gómez-Medina R, Froufe-Pérez LS, López C, Chantada L, Sheffold F, et al. Opt Express 2011;19:4815–26.
- [57] Wheeler MS. [Ph.D. thesis]. University of Toronto, 2010.
- [58] Bohren CF, Huffman DR. Absorption and scattering of light by small particles. New York: Wiley; 2004.
- [59] Palik ED. Handbook of optical constants of solids. San Diego: Academic Press; 1998.
- [60] Box GE, Hunter WG, Hunter JS. Statistics for experimenters. Toronto: John Wiley & Sons; 1978.
- [61] Volokitin AI, Persson BNJ. Phys Rev B 2004;69:045417.
- [62] Basu S, Zhang ZM. J Appl Phys 2009;105:093535.
- [63] Ginn JC, Brener I, Peters DW, Wendt JR, Stevens JO, Hines PF, et al. Phys Rev Lett 2012; 108: 097402.
- [64] Formanek F, Takeyasu N, Tanaka T, Chiyoda K, Ishikawa A, Kawata S. Opt Express 2006;14:800–9.
- [65] Boltasseva A, Shalaev VM. Proc Soc Photo-Opt Ins 2008;1:1–17.
- [66] Zhang S, Fan W, Malloy KJ, Brueck SRJ, Panoiu NC, Osgood RM. J Opt Soc Am B 2006;23:434–8.
- [67] Gor'kov LP. Sov Phys Dokl 1962;6:773.
- [68] Yosioka K, Kawasima Y. Acustica 1955;5:167–73.
- [69] Raeymaekers B, Pantea C, Sinha DN. J Appl Phys 2011;109:014317.